Int. J. Electrochem. Sci., 16 **(2021)** Article Number: 211126, doi: 10.20964/2021.11.16

International Journal of
ELECTROCHEMICAL
SCIENCE
www.electrochemsci.org

Saccharum Officinarum Leaf Extract as Corrosion Inhibitor of Copper Corrosion in Sulphuric Acid Solution: Experiments and Theoretical Calculations

Zhengyuan Gao[1], Pengfei Sun[1], Lianteng Du[1], Xiang Zhang[1], Jialong Bai[1], Haojie Xing[1], Yongbo Yan[2,]*

[1] School of Mechatronics & Vehicle Engineering, Chongqing Jiaotong University, Chongqing, 400074,China;
[2] School of Oil and Natural Gas Engineering, Southwest Petroleum University, Chengdu 610500
[*]E-mail: 779265488@qq.com, yanyongbo0520@163.com

Received: 11 July 2021 / *Accepted:* 30 August 2021 / *Published:* 10 October 2021

Saccharum officinarum leaf extract was obtained by the ethanol soaking method in this study. Fourier infrared spectroscopy experiments show that Saccharum officinarum leaf extract contains a mass of oxygen or nitrogen-containing functional groups. Electrochemical experiments show that Saccharum officinarum leaf extract can efficaciously suppression the corrosion of Cu at H_2SO_4. Polarization curve test shows that the η of Saccharum officinarum leaf extract can reach more than 93%, and it is a mixed-type corrosion inhibitor. The morphology test indicates that after Saccharum officinarum leaf extract is adsorbed onto the Cu interface, the corrosion rate of the corrosive medium on the copper surface is significantly reduced. Quantum chemical (QC) calculations and molecular dynamics (MD) simulations have shown that Saccharum officinarum leaf extract can efficaciously control the corrosion of Cu at sulfuric acid solution.

Keywords: Saccharum officinarum leaf extract; Corrosion inhibitor; H_2SO_4; Copper; Quantum chemical calculations

1. INTRODUCTION

Cu materials and its corresponding alloys have played a vital function at the evolution of human civilization since ancient times [1]. From the bronze sword, bronze mirror, and bronze tripod of the Warring States Period to the copper microelectronics, heat exchanger, ship and other fields in the 21st century. This is all due to the good ductility, conductivity and relative corrosion resistance of copper. However, copper parts and equipments will also be gravely corroded during long-term service, forming a relatively dense oxide film at the copper interface. In order to command the corrosion of copper in sulfuric acid medium, it is often necessary to append a little amount of inhibitor to the corrosive

atmosphere. The inhibitor molecules form a denitrification segregate film at the metal basement to efficaciously command the corrosive medium from further corroding the metal substrate and play an effective role in protecting the metal. Therefore, among abundant metal corrosion defend tools, the inhibitors are favored by abundant of corrosion scientist due to their remarkable effects, simple operation, and remarkable anti-corrosion effects [2].

Organic inhibitor molecules currently incorporate heteroatoms such as N (nitrogen), O (oxygen), S (sulfur), and unsaturated functional groups [3-9]. These unique properties of the corrosion inhibitor molecules are conducive to the formation of a pyknotic and ordered molecular par-close at the metal surface by the corrosion inhibitor molecules, thereby blocking out the corrosion of the corrosive particle on the copper substrate. However, the inhibitor has its own obvious blemish. A mass of inhibitors can bring about serious damage to the ecological system. Therefore, the use of environmentally friendly inhibitor molecules has turn into a consensus among corrosion guard scholars. Common green corrosion inhibitors including amino acids, spices, ionic liquids and nature extracts. Among them, plant extracts are more enthusiastically sought after. Recently, He et al. [10] used an integrate of theoretical calculations and experiments to understand thoroughly the anti-corrosion nature of Artocarpus heterophyllus Lam leaves extract on copper in sulfuric acid solution. Electrochemical experiments show that when the concentrations of Artocarpus heterophyllus Lam leaves extract reaches 500 ppm, its η can reach over 97%. Zhou et al. [11] studied the anti-corrosion mechanism of Syzygium samarangense leaf extract for Q235 steel at sulfuric acid by combining experiments and theoretical calculations. Polarization curve experiment data show that the η of Syzygium samarangense leaf extract can be close to about 90%. Hence, it can be judged that Syzygium samarangense leaf extract can exhibit high-quality anti-corrosion speciality.

In this work, we used the ethanol soaking method to obtain Saccharum officinarum leaf extract. We used QC, MD, polarization curve analysis, electrochemical impedance spectroscopy tests, atomic force microscopy to explore the anti-corrosion mechanism of Saccharum officinarum leaf extract on copper.

2. EXPERIMENTAL METHOD

2.1. Preparation of Saccharum officinarum leaf extract

Collect the dried Saccharum officinarum leaf, and crush the Saccharum officinarum leaf into powder with a grinder. Pour the powdered Saccharum officinarum leaf into a beaker of absolute ethanol. After immersing for 48 hours, the supernatant was taken out and poured into a rotary evaporating flask. Spin drying in a rotary evaporator to obtain the Saccharum officinarum leaf extract required for our experiment. Then, the obtained Saccharum officinarum leaf extract was detected to Fourier infrared spectroscopy (Nicolet iS50). The range of Fourier infrared spectroscopy test is 500 cm^{-1} to 4000 cm^{-1}.

2.2. Preparation of electrode materials and solutions

Copper electrode ($1 \times 1 \times 1$ cm^3) is airtight via epoxy resin, revealing only one interface to be measured. Before the electrochemical test, the Cu electrodes were polished on 180 to 3000 # sandpaper. The 0.5 M sulfuric acid solution is made of 98% concentrated sulfuric acid and ultrapure water.The obtained Saccharum officinarum leaf extract was separately dissolved in 0.5 M H_2SO_4 solution to prepare corroson solutions with concentrations of 100 mg/L, 200 mg/L, 300 mg/L, 400 mg/L, and 500 mg/L.

2.3. Surface topography analysis

The pure copper used in this experiment is the sample to be tested.The copper sample is cut into $0.1 \times 1 \times 1$ cm^3 chunks for AFM testing (MFP-3D-BIO). Before the surface test, the copper chunks were polished at 180 to 5000 # sandpaper. The shined copper chunks were immersed in a 0.5 M H_2SO_4 solution containing and without 500 mg/L Saccharum officinarum leaf extract for 20 h at 298 K.

2.3. Electrochemical tests

The electrochemical experiment in this study was determined to use a standard three-electrode system. Pure copper is the working electrode. The saturated calomel electrode is the reference electrode. The platinum electrode is the counter electrode.First, perform an open circuit potential test, soak the Cu electrode at the test solution for half an hour to ensure that the interface of the Cu electrode has arrived a stabilized state. Then carry out electrochemical impedance spectroscopy test, the initial voltage when the open circuit potential is measured is a jar-less value of OCP, and the excitation signal is a voltage of 10 millivolts. The frequency section of the experiment is from 100000 Hz to 0.01 Hz. The test section of the polarization curve is *Eocp* ± 0.25 V, and the scan rate is 1 mV/s [12-14].

2.5. Calculation details

We used Materials Studio (MS) software to verdict the properties of Saccharum officinarum leaf extract. The computational tasks is Geometry Optimization, the Functional is GGA and PBE. The adsorption of Saccharum officinarum leaf extract at the Cu (111) interface was counted using MS software. Firstly, we create a Cu (111) vacuum layer. Then this vacuum stratum was padding with 400 H_2O molecules and a Saccharum officinarum leaf extract molecule. The Dynamics was calculated task, the Time step was1fs, and the total calculation time was 2000 ps.

3. RESULTS AND DISCUSSION

3.1. FTIR research

Figure 1 is the Fourier infrared spectrum of Saccharum officinarum leaf extract. 3296.5 cm^{-1} is related to O-H or N-H stretching. 2918 cm^{-1} peak is related to C-H stretching vibration. 1583 cm^{-1} peak

is related to C=O or C=N stretching vibration. 1375 cm^{-1} peak is related to CH_3 stretching vibration. The peak at 1046 cm^{-1}, which is attributed to the C-O or C-N stretching vibration.

Besides, we consult the references of Saccharum officinarum leaf ingredients[15-18]. It can be found that Saccharum officinarum leaf contains 3-(4-hydroxy-3-methoxyphenyl)acrylic acid (HMA), 1-methyl-3-nitrosoguanidine (MND), 3-(3,4-dihydroxyphenyl)acrylic acid (DDA), 5,7-dihydroxy-2-(4-hydroxyphenyl)-4H-chromen-4-one (DHC). Figure 2 presents the chemical structural formulas of the four components, respectively. Therefore, we can judge that Saccharum officinarum leaf has the potential of an excellent corrosion inhibitor.

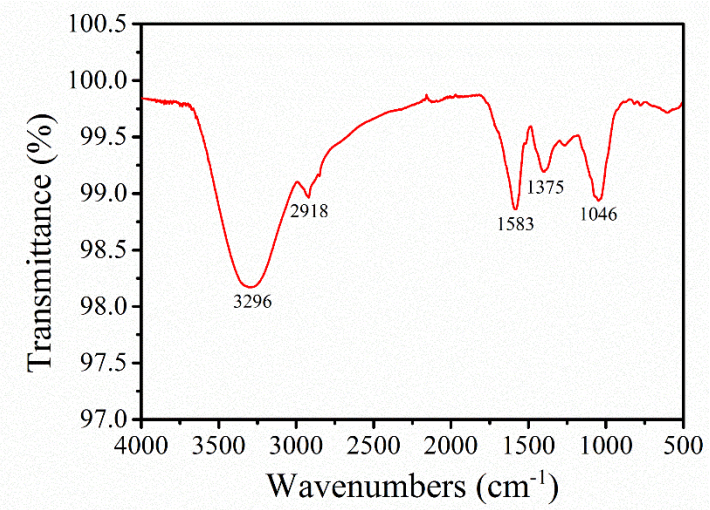

Figure 1. Fourier infrared spectrum (FTIR) of Saccharum officinarum leaves extract.

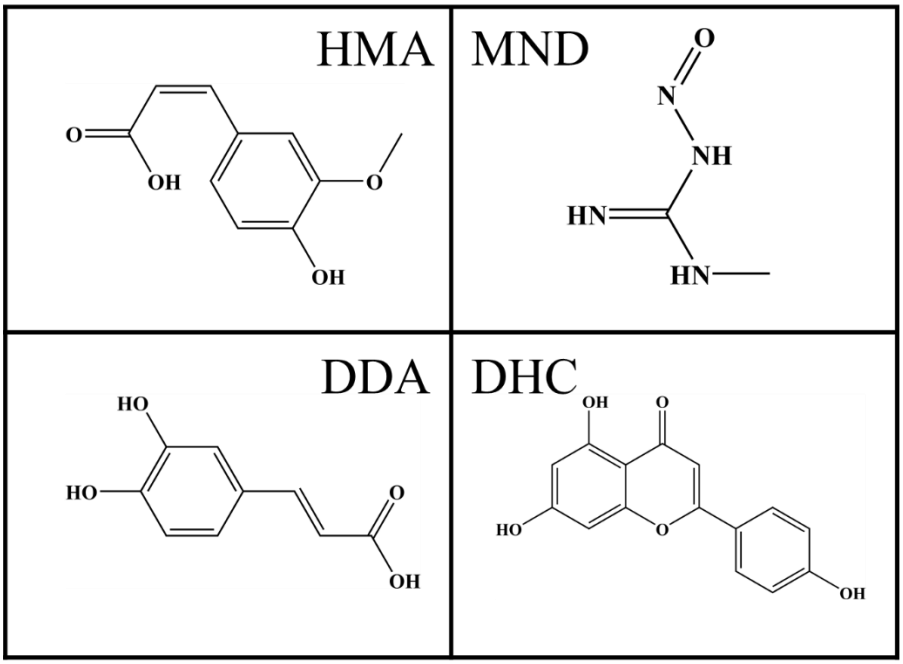

Figure 2. The molecular structure of the 4 primary components of Saccharum officinarum leaf extract.

3.2. Potentiodynamic Polarization curve analysis

Figure 3 shows the polarization curves of Cu electrodes immersed in 0.5 mol/L sulfuric acid solution containing diverse concentrations of Saccharum officinarum leaves extract. It can be clearly found that as the concentration of Saccharum officinarum leaves extract augments, the i_{corr} shows a downward status. This indicates that Saccharum officinarum leaves extract formed a pyknotic protective film at the copper surface [19]. Besides, the branches of the cathode showed a parallel condition, which indicated that the adsorption of Saccharum officinarum leaf extraction on the copper interface did not alter the reactive mechanism of the cathode [3, 10, 20]. In order to quantitatively analysis the anti-corrosion peculiarity of Saccharum officinarum leaves extract, we used Tafel extrapolation to gain the corresponding polarization curve data. The fitted data are appeared in Table 1. The i_{corr} value of the copper surface in the blank solution is 19.1 μA cm^{-2}. After adding Saccharum officinarum leaf extraction, the i_{corr} obviously shows a downward trend. When the concentration of Saccharum officinarum leaf extraction is 500 mg/L, its η is 93.6%. The η is calculated by the formula (1) [21-26]:

$$\eta(\%) = \frac{i_{corr,0} - i_{corr}}{i_{corr,0}} \times 100 \qquad (1)$$

where $i_{corr,\,0}$ and i_{corr} indicate the corrosion current density of without and with Saccharum officinarum leaves extract, respectively. It is also worth noting that before and after adding Saccharum officinarum leaves extract, the change in corrosion potential was visibly less than 85 millivolt. Therefore, it can be judged that Saccharum officinarum leaf extraction is a mixed inhibitor [27-30]. The reaction of the cathodic and anodic of the Cu electrode can be suppressed at the same time.

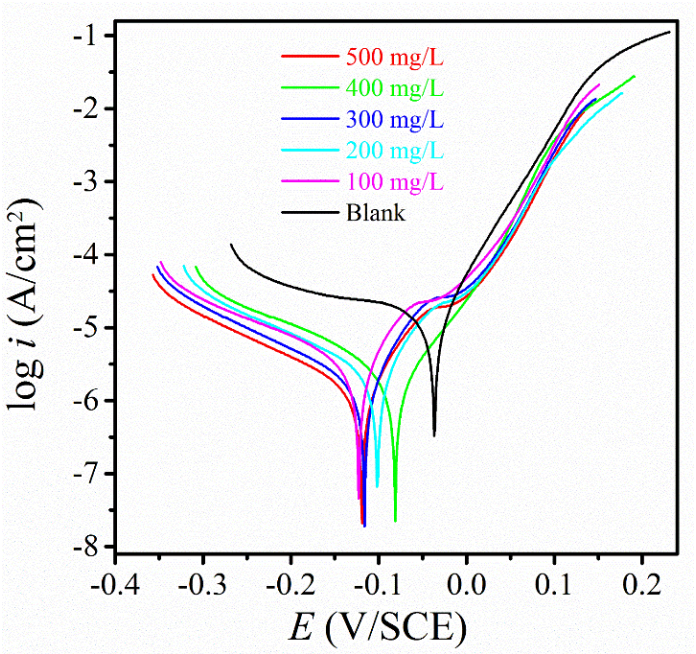

Figure 3. Polarization curves of Cu electrodes immersed in 0.5 M H_2SO_4 solution containing various concentrations of Saccharum officinarum leaves extract at 298 K.

Table 1. Polarization curve data of Cu electrodes immersed in 0.5 M H_2SO_4 solution containing various concentrations of Saccharum officinarum leaves extract at 298 K.

C (mg/L)	E_{corr}(mV/SCE)	i_{corr}(μA cm^{-2})	β_c(mV dec^{-1})	β_a(mV dec^{-1})	η(%)
Blank	–37	19.1	–238	78	—
100	–123	4.52	–181	65	76.3
200	–102	2.58	–166	83	86.5
300	–116	1.68	–174	60	91.2
400	–81	1.39	–167	68	92.7
500	–119	1.22	–154	86	93.6

3.3. EIS

Figure 4 (a) and (b) respectively show the Niqust plot and Bode map of Cu electrodes immersed in 0.5 M sulfuric acid solution containing various concentrations of Saccharum officinarum leaves extract. In Figure 4(a), it can be clearly found that when the concentration of the blank solution and Saccharum officinarum leaves extract is low (100 mg/L), there is obvious Warburg impedance in the low frequency district, which is caused by the diffusion of copper ions after corrosion of the copper interface into the bulk solution [23, 31]. When the concentration of Saccharum officinarum leaves extract is low, the protective film formed by Saccharum officinarum leaves extract on the copper surface is not dense enough.

When the concentration of Saccharum officinarum leaves extract increases, it can be clearly found that the Warburg impedance in the low frequency region has disappeared, which indicates that Saccharum officinarum leaves extract forms a pyknotic protective scherm at the Cu surface, thereby inhibiting the corrosion of the Cu surface [20, 27].

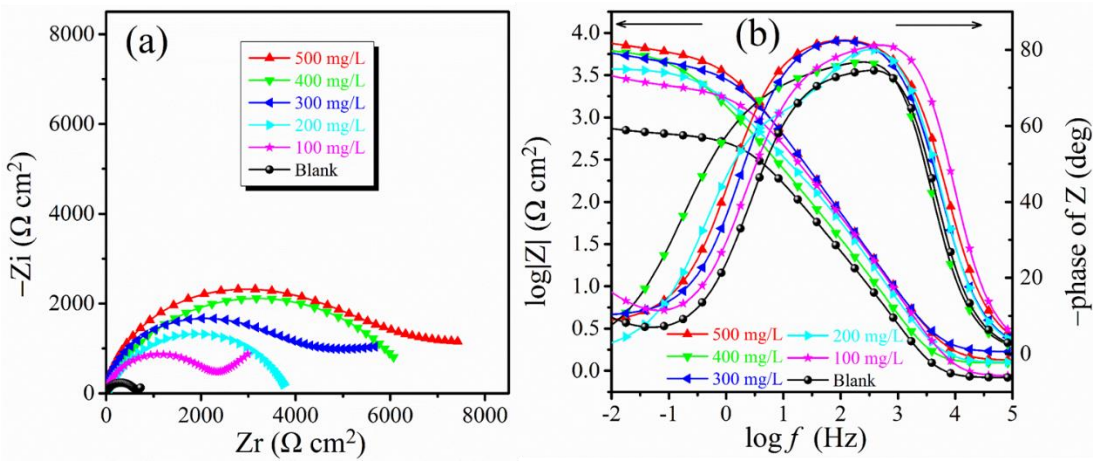

Figure 4. EIS of copper electrodes immersed in 0.5 M H_2SO_4 solution containing various concentrations of Saccharum officinarum leaves extract: (a) Niqust plot, (b) Bode plot.

Besides, as the concentration of Saccharum officinarum leaves extract increases, the charge transfer resistance in the high-frequency section increases overtly, which manifests that the protective scherm formed by Saccharum officinarum leaf extraction on the surface of the copper electrode inhibits the corrosion of the corrosive medium on the copper electrode [19, 23]. In Figure 4(b), it can be clearly found that after adding Saccharum officinarum leaves extract, the phase angle diagram and impedance modulus diagram clearly show an increasing status, which indicates that Saccharum officinarum leaves extract is a good inhibitor.The Figure 5 (equivalent circuit diagram) is used to fit the EIS data. Table 2 is the EIS data. The formula of η is obtained by using the following formula [20, 32-34]:

$$\eta(\%) = \frac{R_P - R_{P,0}}{R_p} \times 100 \qquad (2)$$

where R_p and $R_{p,0}$ stand for the polarization resistance in the presence and absence of Saccharum officinarum leaves extract, respectively. In Table 2, it can be found that the Saccharum officinarum leaf extraction is 500 ppm, the η of Saccharum officinarum leaf extraction is 92.3%. Besides, as the concentrations of Saccharum officinarum leaves extract increases, the electric double layer capacitance and the membrane capacitance show a decline status. This shows that Saccharum officinarum leaf extraction replaced the water molecules at the Cu surface to form a pyknotic protective scherm [35].

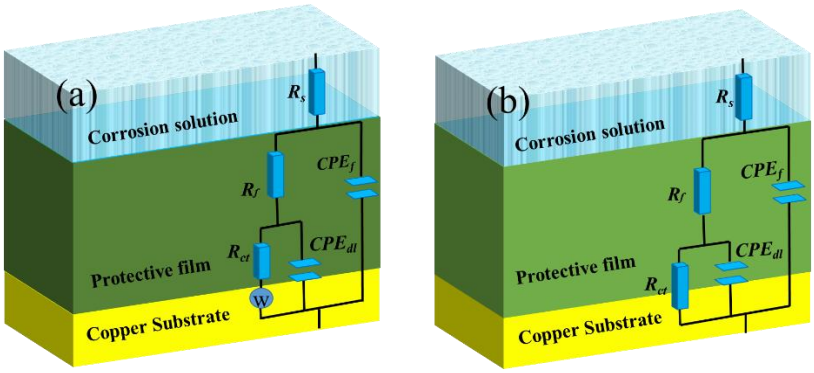

Figure 5. The most suitable equivalent circuit diagram for fitting EIS data.

Table 2. Eis fitting data of copper electrodes immersed in 0.5 M H_2SO_4 solution containing various concentrations of Saccharum officinarum leaves extract.

C	R_f	R_{ct}	R_p	C_f	n_1	C_{dl}	n_2	W	η (%)
(mg/L)	(kΩ cm^2)	(kΩ cm^2)	(kΩ cm^2)	(μF cm^{-2})		(μF cm^{-2})		(×10^{-2} Ω cm^2 s$^{1/2}$)	
Blank	0.02	0.54	0.56	137.2	1	110.5	0.72	2.4	—
100	0.09	2.15	2.24	77.1	1	83.2	0.68	3.4	75.0
200	0.25	3.59	3.84	66.1	0.97	72.5	0.71	—	85.4
300	0.44	5.13	5.57	53.2	0.94	68.3	0.72	—	89.5
400	0.47	6.59	7.06	44.1	1	52.4	0.66	—	91.8
500	0.51	6.81	7.32	40.7	0.8	43.9	0.94	—	92.3

3.4. AFM research

Figure 6 presents the surface feature of Cu electrodes immersed in H_2SO_4 solution with and without 500 mg/L Saccharum officinarum leaves extract. In Figure 6(a), the surface topography of a Cu block immersed in a 0.5 M sulfuric acid solution containing 500 ppm Saccharum officinarum leaves extract for 20 hours is at a temperature of 298 K. Figure 6(b) is a 3D morphology of the Cu electrode immersed in 0.5 mol/L sulfuric acid solution. The surface of the copper sample has been gravely corroded without corrosion inhibitor. The corrosion holes are very deep, and there are mountain-like corrosion scallops at the Cu surface throughout the test. This shows that corrosive media such as sulfuric acid strongly damaged the surface of the copper sample. The copper surface in Figure 6(a) is still smooth and clean, which strongly proves that Saccharum officinarum leaves extract can adsorb at the Cu interface and inhibit the corrosion of the Cu surface.

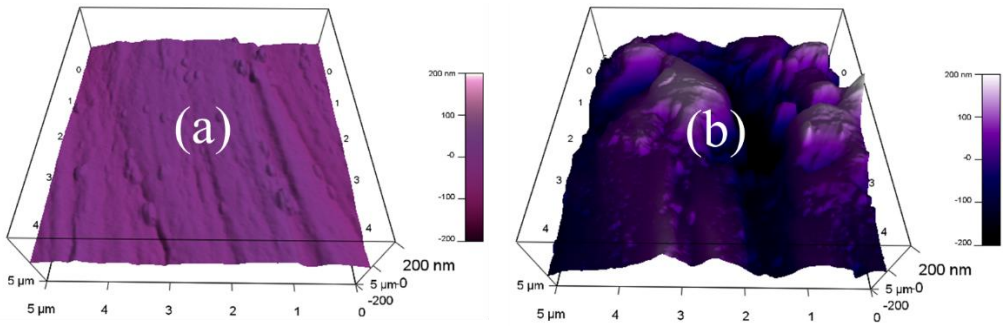

Figure 6. Atomic force microscope images under different experimental conditions; (a) the surface topography of a Cu block immersed in a 0.5 M sulfuric acid solution containing 500 ppm Saccharum officinarum leaves extract for 20 hours is at a temperature of 298 K. (b) Cu electrode immersed in 0.5 mol/L sulfuric acid.

3.5. Theoretical calculation research

Figure 7 shows the optimized molecular configurations of the four substances HMA, MND, DDA, and DHC, and the corresponding electrostatic potential diagrams. It can be clearly found that the optimized molecular structures of HMA, MND, DDA, and DHC are basically on the same plane, which indicates that HMA, MND, DDA, and DHC can be adsorbed at the copper interface in parallel to obtain a stable configuration.

In addition, we can find that the electrostatic potential diagrams of HMA, MND, DDA, and DHC are formed of red and blue section. The red area indicates that the molecule has nucleophilic nature, and the blue area indicates that the molecule has electrophilic nature [35, 36]. It can be found that the red regions in HMA, MND, DDA, and DHC are mainly around the N atoms and O atoms, which indicates that these regions can provide electron and form coordination bond with copper.

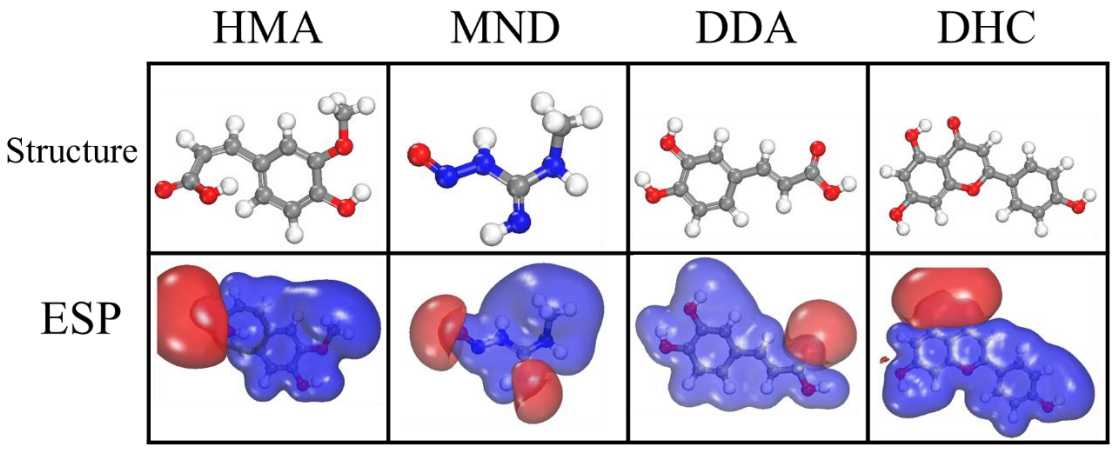

Figure 7. The optimized structure and electrostatic potential diagrams of HMA, MND, DDA and DHC.

Figure 8 is the electrons cloud distribute diagram of the frontline molecular orbitals of HMA, MND, DDA, and DHC. The HOMO orbital is corresponds to the electron-donating capacity, and the LUMO orbital is corresponds to the electron-donating capacity [31, 37-39]. It can be clearly found in Figure 8 that the electrons clouds of HOMO orbitals of HMA, MND, and DDA are basically uniformly distributed throughout the molecule, which indicates that these molecules are more easily to give electrons to form coordination bond with copper. The LUMO orbital indicates that the inhibitor easily accepts electrons from the copper interface to form a couple back bond, thereby adsorbing on the copper surface.

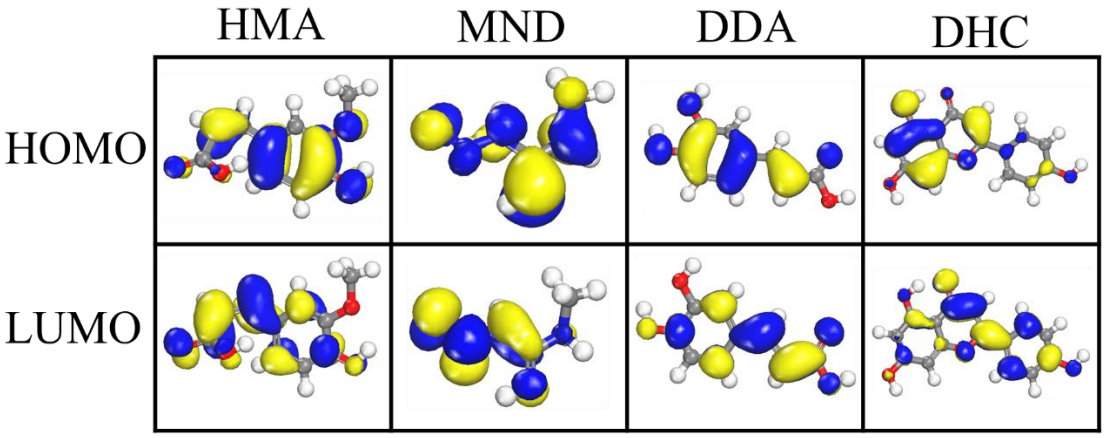

Figure 8. HMA, MND, DDA and DHC front-line molecular orbital distribution map.

Figure 9 presents the μ and ΔE values of HMA, MND, DDA and DHC. Most corrosion workers believe that when the corrosion inhibitor molecule has a large dipole value, it is easier to alter the C_{dl} of the metal surface by adsorbing at the Cu surface [40-42]. This facilitates the adsorption of corrosion

inhibitor molecules at the Cu surface. The μ values of HMA, MND, DDA and DHC are 7.53 D, 3.63 D, 1.67 D and 6.21 D, respectively. Therefore, it can be judged that HMA and DHC have higher corrosion inhibition performance than the other two substances. Figure 9 (b) shows the energy gap values of HMA, MND, DDA and DHC. We can clearly see that the LUMO orbital values of the four substances are very close. However, the HOMO orbital value is very different, and the HOMO value of MND is the smallest. Therefore, we can effectively judge that the corrosion inhibition effect of MND is the smallest.

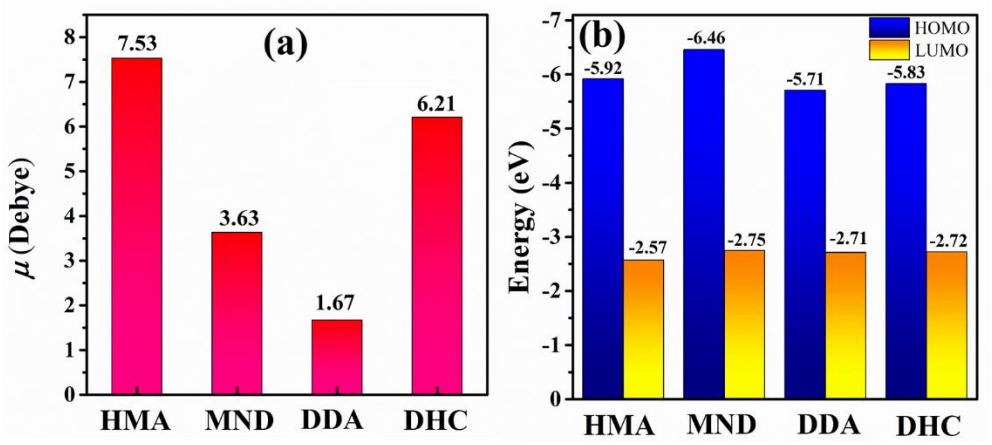

Figure 9. The μ values and ΔE values of HMA, MND, DDA and DHC.

3.6. Theoretical calculation research

Figure 10 shows the stable configuration of HMA, MND, DDA and DHC after adsorption on Cu(111) surface. It can be clearly found that HMA, MND, DDA and DHC basically use a parallel adsorption method to act at the Cu interface to obtain the maximum coverage. Their adsorption energy at the copper interface can be calculated by the formulas (3) and (4) [43-45]:

$$E_{binding} = -E_{interact} \quad (3)$$

$$E_{interact} = E_{tot} - (E_{subs} + E_{inh}) \quad (4)$$

where E_{tot} is the total energy of the whole simulation system, E_{sub} stands for the total energy of 400 H_2O molecules and Cu (111) substrate, and E_{inh} is the energy of researched molecule. The binding energies of HMA, MND, DDA and DHC on the copper surface are 356.1 kJ/mol, 180.9 kJ/mol, 422.1 kJ/mol, and 526.3 kJ/mol. The binding force of DHC on the Cu(111) surface is the strongest.

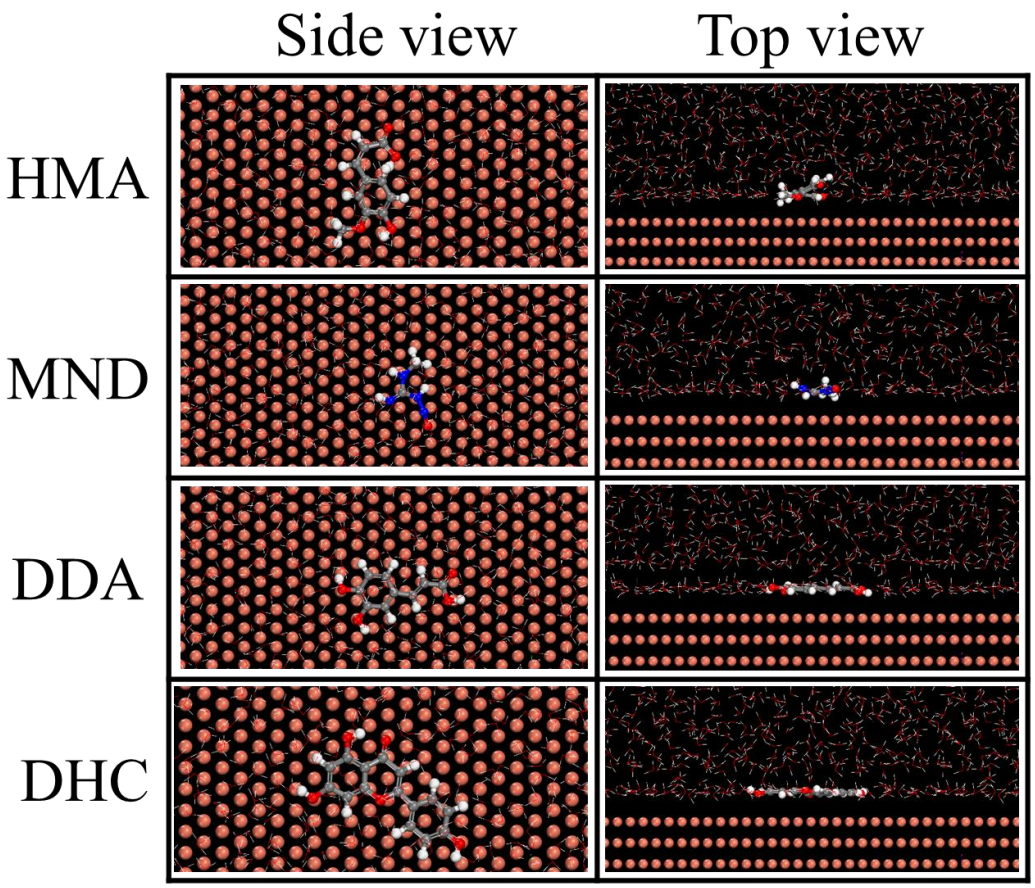

Figure 10. The jarless adsorption configurations of HMA, MND, DDA and DHC on the copper surface.

3.7. Adsorption isotherm model research

In order to study the adsorption mechanism of Saccharum officinarum leaf extract on the copper surface, The different adsorption equations are used to fit the polarization curve. The linear regression coefficients (R^2) after fitting manifest that the adsorption of Saccharum officinarum leaf extract at the copper surface accords with the Langmuir single-layer adsorption. Its expression is as follows [19]:

$$\frac{C}{\theta} = \frac{1}{K_{ads}} + C \qquad (5)$$

where C is the concentrations of Saccharum officinarum leaf extract. η indicates the surface coverage. K_{ads} is the adsorption equilibrium constant. In order to further determine the adsorption type of Saccharum officinarum leaf extract on the copper surface. We use formula 6 to calculate [46]:

$$K_{ads} = \frac{1}{1000}\exp(-\frac{\Delta G^0_{ads}}{RT}) \qquad (6)$$

The calculated K_{ads} and ΔG^0_{ads} values are listed in Figure 11. The large K_{ads} value indicates that Saccharum officinarum leaf extract can be strongly adsorbed at the Cu interface. The value of ΔG^0_{ads} is between –20 to –40 kJ/mol, which manifests that the adsorption of Saccharum officinarum leaf extract on the copper surface simultaneously exists physical and chemical adsorption [3, 42, 47].

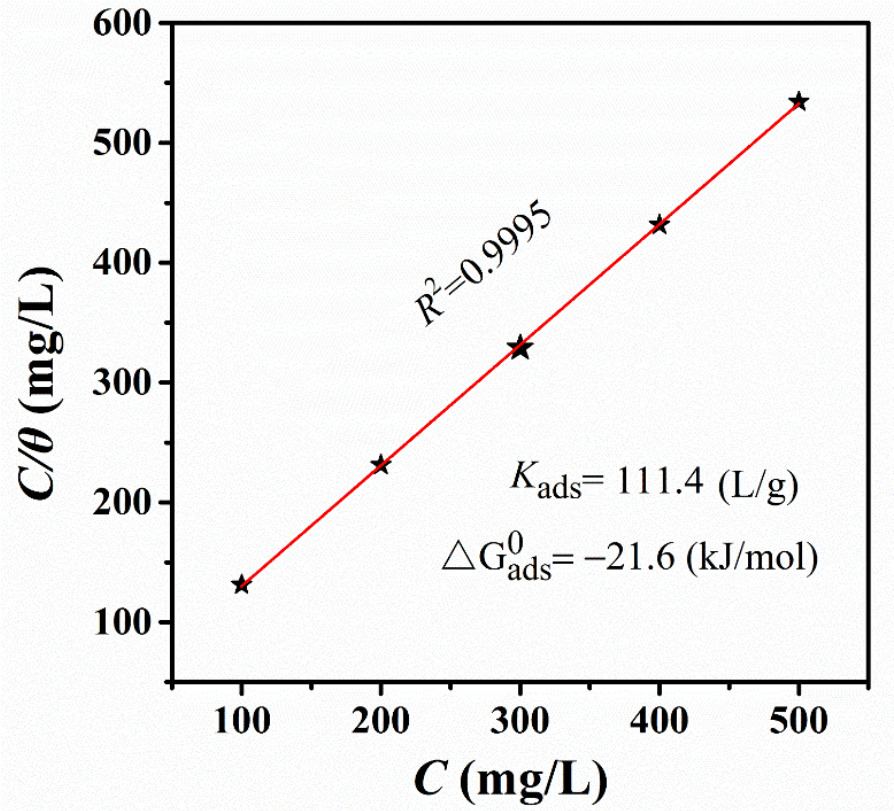

Figure 11. Langmuir adsorption isotherm.

4. CONCLUSIONS

Saccharum officinarum leaf extract obtained by pure immersion extraction method contains a large amount of nitrogen and oxygen heteroatom functional groups. Electrochemical experiment results show that Saccharum officinarum leaf extract can exhibit high anti-corrosion peculiarity, and it can inhibit the reaction of the copper electrode cathode and anode at the same time, which is a mixed-type inhibitor. The surface morphology test strongly proved that Saccharum officinarum leaf extract can be adsorbed onto the Cu surface, thereby command the copper corrosion. In addition, QC and MD have proved that the four substances in Saccharum officinarum leaf extract can exhibit high corrosion inhibition performance. The isotherm model study indicate that the adsorption of Saccharum officinarum leaf extract on the Cu surface accords with the Langmuir adsorption, and there are both physical and chemical adsorption.

References

1. Ž.Z. Tasić, M.B. Petrović Mihajlović, M.B. Radovanović, A.T. Simonović, and M.M. Antonijević, *J. Mol. Struct*., 1159 (2018) 46.
2. Ž.Z. Tasić, M.B. Petrović Mihajlović, M.B. Radovanović, and M.M. Antonijević, *J. Mol. Liq.*, 265 (2018) 687..

3. X. Zuo, W. Li, W. Luo, X. Zhang, Y. Qiang, J. Zhang, H. Li, and B. Tan, *J. Mol. Liq.*, 321 (2021) 114914.
4. F. Bahremand, T. Shahrabi, and B. Ramezanzadeh, *J. Colloid Interf. Sci.*, 582 (2021) 342.
5. M.B. Petrović Mihajlović, M.B. Radovanović, Ž.Z. Tasić, and M.M. Antonijević, *J. Mol. Liq*., 225 (2017) 127..
6. S. Y. Al-Nami, *Int. J. Electrochem. Sci*., 14 (2019) 3986.
7. S. Xu, W. Li, X. Zuo, D. Zheng, X. Zheng, and S. Zhang, *Int. J. Electrochem. Sci*., 14 (2019) 5777.
8. C. Wang, W. Gou, C. Liu, D. Fu, L. Zhou, C. Lai, B. Xie, and S. Zhu, *Int. J. Electrochem. Sci.*, 14 (2019) 3443.
9. A. S. Fouda, M. Abdel Azeem, S.A. Mohamed, A. El-Hossiany, and E. El-Desouky, *Int. J. Electrochem. Sci*., 14 (2019) 3932.
10. J. He, Q. Xu, G. Li, Q. Li, R. Marzouki, and W. Li, *J. Ind. Eng. Chem*., 102 (2021) 260.
11. Y. Zhou, C. Zhu, S. Xu, B. Xiang, and R. Marzouki, *J. Ind. Eng. Chem*., 102 (2021) 302.
12. B. Tan, J. He, S. Zhang, C. Xu, S. Chen, H. Liu, and W. Li, *J. Colloid Interf. Sci*., 585 (2021) 287.
13. X. Ren, S. Xu, X. Gu, B. Tan, J. Hao, L. Feng, W. Ren, F. Gao, S. Zhang, Y. Xiao, and L. Huang, *J. Colloid Interf. Sci*., 585 (2021) 614.
14. Q.H. Zhang, B.S. Hou, and G.A. Zhang, *J. Colloid Interf. Sci*., 572 (2020) 91.
15. B. Wang, P. Duh, S. Wu, and M. Huang, *Food Chem*., 124 (2011) 495-500.
16. J.C.P. Penteado, J.C. Masini, *Analytical Lett*., 42 (2009) 2747-2757.
17. D.A. Sampietro, M.A. Vattuone, and M.I. Isla, *J. Plant Physiol*., 163 (2006) 837-846.
18. P. Georges, M. Sylvestre, H. Ruegger, and P. Bourgeois, *Steroids*., 71 (2006) 647-652.
19. Y. Qiang, L. Guo, H. Li, and X. Lan, *Chem. Eng. J*., 406 (2021) 126863.
20. B. Tan, S. Zhang, Y. Qiang, W. Li, H. Liu, C. Xu, and S. Chen, *J. Mol. Liq*., 286 (2019) 110891.
21. T. Yan, S. Zhang, L. Feng, Y. Qiang, L. Lu, D. Fu, Y. Wen, J. Chen, W. Li, and B. Tan, *J. Taiwan Inst. Chem. E*., 106 (2020) 118.
22. B. Tan, S. Zhang, Y. Qiang, W. Li, H. Li, L. Feng, L. Guo, C. Xu, S. Chen, and G. Zhang, *J. Mol. Liq*., 298 (2020) 111975.
23. Y. Qiang, S. Zhang, and L. Wang, *Appl. Surf. Sci*., 492 (2019) 228-238.
24. Z.Z. Tasic, M.M. Antonijevic, M.B. Petrovic Mihajlovic, and M.B. Radovanovic, *J. Mol. Liq*., 219 (2016) 463-473.
25. X. Wang, H. Jiang, D. Zhang, L. Hou, and W. Zhou, *Int. J. Electrochem. Sci*., 14 (2019) 1178-1196.
26. A. S. Fouda, M.M. Hegazi, and A. El-Azaly, *Int. J. Electrochem. Sci.*, 14 (2019) 4668-4682.
27. B. Tan, B. Xiang, S. Zhang, Y. Qiang, L. Xu, S. Chen, and J. He, *J. Colloid Interf. Sci.*, 582 (2020) 918-931.
28. J. Zhang, *Int. J. Electrochem. Sci*., 15 (2020) 1437-1449.
29. S. Tao, H. Huang, *Int. J. Electrochem. Sci*., 14 (2019) 5435-5447.
30. J. Tang, Y. Hu, H. Wang, Y. Zhu, Y. Wang, Z. Nie, and Y. Wang, *Int. J. Electrochem. Sci*., (2019) 2246-2264.
31. Y. Qiang, H. Li, and X. Lan, *J. Mater. Sci. Technol*., 52 (2020) 63-71.
32. Y. Qiang, S. Zhang, H. Zhao, B. Tan, and L. Wang, *Corros. Sci*., 161 (2019) 108193.
33. J. Liu, Y. Zhou, C. Zhou, and H. Lu, *Int. J. Electrochem. Sci*., 15 (2020) 2499 – 2510.
34. N. V. Likhanova, P. Arellanes-Lozada, O. Olivares-Xometl, I.V. Lijanova, J. Arriola-Morales, J.C. Mendoza-Hérnandez, and G. Corro, *Int. J. Electrochem. Sci*., 14 (2019) 2655-2671.
35. L. Gao, S. Peng, X. Huang, and Z. Gong, *Appl. Surf. Sci.*, 511 (2020) 145446.
36. B. Tan, S. Zhang, H. Liu, Y. Qiang, W. Li, L. Guo, and S. Chen, *J. Taiwan Inst. Chem. E*., 102 (2019) 424–437.
37. B. Tan, S. Zhang, H. Liu, Y. Guo, Y. Qiang, W. Li, L. Guo, C. Xu, and S. Chen, *J. Colloid Interf. Sci*., 538 (2019) 519-529.
38. S. Chen, B. Zhu, and X. Liang, *Int. J. Electrochem. Sci*., 15 (2020) 1-15.
39. W. Luo, W. Li, J. Tan, J. Liu, B. Tan, X. Zuo, Z. Wang, and X. Zhang, *J. Mol. Liq*., 314 (2020)

113630.
40. B. Tan, S. Zhang, W. Li, X. Zuo, Y. Qiang, L. Xu, J. Hao, and S. Chen, *J. Ind. Eng. Chem.*, 77 (2019) 449-460.
41. Y.J. Yang, Y. Li, L. Wang, H. Liu, D.M. Lu, and L. Peng, *Int. J. Electrochem. Sci*., 14 (2019) 3375-3392.
42. J. He, D. Yu, Q. Xu, G. Li, G. Chen, J. An, J. Yang, and W. Li, *J. Mol. Liq*., 325 (2021) 115145.
43. B. Tan, S. Zhang, Y. Qiang, L. Guo, L. Feng, C. Liao, Y. Xu, and S. Chen, *J. Colloid Interf. Sci*., 526 (2018) 268-280.
44. H. Li, Y. Qiang, W. Zhao, and S. Zhang, *Corros. Sci*., 191 (2021) 109715.
45. Z. Xiao, Z. Zhou, L. Song, D. Wu, C. Zeng, Z. Cao, *Int. J. Electrochem. Sci*., 14 (2019) 4705-4717.
46. B. Tan, S. Zhang, Y. Qiang, L. Feng, C. Liao, Y. Xu, and S. Chen, *J. Mol. Liq*., 248 (2017) 902-910.
47. I. Martinović, G. Zlatić, Z. Pilić, L. Šušić, O. Kowalska, D. Petrović, F. Falak, and J. Mišković, *Int. J. Electrochem. Sci*., 14 (2019) 4206-4215